Homogeneous Cu_2O p-n junction photocathodes for solar water splitting

Tuo Wang, Yijia Wei, Xiaoxia Chang, Chengcheng Li, Ang Li, Shanshan Liu, Jijie Zhang, Jinlong Gong*

Key Laboratory for Green Chemical Technology of Ministry of Education, School of Chemical Engineering and Technology, Collaborative Innovation Center of Chemical Science and Engineering, Tianjin University, Tianjin 300072, China

ARTICLE INFO

ABSTRACT

Cu_2O is considered as one of the most promising p-type semiconductors for photocathodes in solar water splitting due to its abundance, nontoxicity and appropriate band gap of 2.0 eV with favorable energy band positions. It has been long desired to find a proper n type semiconductor for p-Cu_2O to form a p-n junction to generate a more positive onset potential. However, most previous research adopted heterogeneous p-n junctions due to the difficulty in obtaining n-type Cu_2O, and the utilization of p-n Cu_2O homojuncion was limited to solid-state photovoltaic devices. This paper describes a facile electrodeposition process for n-type Cu_2O to construct the homogenous p-n junction, which is further protected by TiO_2 for water splitting, demonstrating the possibility of applying Cu_2O p-n homojunction in an aqueous condition for the first time. Compared with the heterogeneous Schottky junction counterpart, this p-n homojunction significantly increases the built-in potential for efficient charge separation, which leads to an anodic onset potential shift from 0.3 V to 0.7 V versus the reversible hydrogen electrode (RHE), reaching a photocurrent of 4.30 mA/cm^2 at 0 V vs. RHE under AM1.5G. The performance of this electrodeposited p-n Cu_2O photocathode without using the expensive Au back contact is comparable to the most efficient Cu_2O photocathodes reported previously.

1. Introduction

Cuprous oxide (Cu_2O) has been considered to be a promising candidate for high-efficient low cost p-type semiconductor in photoelectrochemical water splitting [1]. Although Cu_2O can generate a photovoltage up to 0.8 V in a non-aqueous system [2], the performance of this photocathode in aqueous electrolyte is far below expectation because of its instability that prevents the direct contact between Cu_2O and electrolyte to form a solid-liquid junction, as well as the difficulty in forming high-quality buried junctions, with only a few encouraging reports.

The pioneering work has shown that atomic layer deposition (ALD) grown aluminum doped zinc oxide (AZO) could form a buried junction with Cu_2O to generate photovoltage in aqueous electrolyte [1]. Although being effective, AZO forms a Schottky junction with p-Cu_2O, which means relatively close Fermi level positions and the existence of interface defects. The theoretical Fermi level offset between ZnO (4.2 eV versus vacuum level) and Cu_2O (4.9 eV versus vacuum level) is estimated to be 0.7 V [3], which largely limits the possible separation of the quasi-Fermi levels upon illumination for photovoltage generation. In addition, the actual band bending at the Cu_2O/AZO Schottky junction is far below 0.7 V due to the pinning of Fermi level caused by

interface defects [4]. Thus, many recent studies focus on finding proper n-type semiconductors to form p-n junctions with p-Cu_2O to generate larger photovoltage.

The n-type material of the p-n heterojunction should have a suitable conduction band alignment and high-quality interface with the p-Cu_2O layer. In practice, however, the choice of this n-type material is not so straightforward since the band alignment is rarely ideal and the existence of interface defects is inevitable [5]. Delaunay and co-workers introduced a thin Ga_2O_3 as a n-type layer that forms a p-n junction with Cu_2O to improve the performance of Cu_2O-based photocathodes [6]. This Cu_2O-Ga_2O_3 p-n junction reduces the conduction band discontinuity along the interface, thus achieving an extremely positive onset potential of 1.02 V and a high cathodic photocurrent of −2.95 mA/cm^2 at 0 V vs. RHE. Wang and co-workers prepared a thin ZnS n-type layer to form a high quality interface with Cu_2O to increase the photovoltage to 0.72 V [7]. ZnS has a reported conduction band position of 3.9 eV versus vacuum level which lies close to its Fermi level [8]. Therefore the Fermi level offset of Cu_2O/ZnS is expected to be 1.0 eV. These p-Cu_2O/n-type semiconductor junctions outperforms the p-Cu_2O/AZO Schottky junctions, confirming the importance of n-type oxide for p-Cu_2O to generate photovoltage and improve the solar energy conversion efficiency. However, it is very likely that defects still

---

exist at the interface of heterogeneous Cu_2O/n-type semiconductor junctions [5]. The lattice mismatch between the crystal structures of different materials can increase charge recombination and hamper the photovoltage and photocurrent. Thus it can be inferred that although many previous research has demonstrated the success in forming heterogeneous p-n or Schottky junctions [1,6,7], homogeneous Cu_2O p-n junction is still highly desired.

The homogeneous Cu_2O p-n junction offers unique advantages compared to heterojunctions. (I) The electron affinity of p-Cu_2O and n-Cu_2O is approximately equal to each other, thus decreasing the conduction band discontinuity along the interface [9,10]. (II) It is possible to form a high quality interface at the junction with similar lattice spacing. However, there is scant research to construct Cu_2O homojunctions due to the lack of reliable methods to produce n-Cu_2O. Cu_2O is an intrinsic p-type semiconductor with a low electron affinity of 3.2 eV. It is often challenging to transfer materials with such a low electron affinity to n-type due to self-compensation by intrinsic defects [11]. Although the success in forming n-Cu_2O is limited, the electrodeposited n-Cu_2O thin films have been reported [12,13]. The strong Cu^{2+} absorption on the unstable surface states caused by the Cu vacancies of Cu_2O can form an inversion layer and transform the conductivity from p to n type [14]. So far, the Cu_2O p-n homojunction has been limited to solar cells, which is thought to be a way to reach the theoretical efficiency of 12% [5]. However, the n-Cu_2O contains a higher degree of lattice disorder with oxygen deficiency [14], which could be easily compensated by absorption of oxygen or water molecules [15]. Thus n-Cu_2O is extremely unstable. The stability of n-Cu_2O is expected to be worse than p-type Cu_2O, while the instability of the latter one in aqueous solutions is already a big problem, which originates from its redox potentials lying within its bandgap [16]. Although ALD-grown TiO_2 protective layers have been proven effective for p-Cu_2O [1,17,18], applying n-Cu_2O in aqueous electrolyte as the photocathode remains a great challenge.

In this work, we report a homogeneous Cu_2O p-n junction for solar water splitting in an aqueous environment for the first time, where the n-Cu_2O layer was fabricated by a facile electrodeposition method. By comparing the carrier lifetimes and photoelectrochemical performance between the homojunction and p-Cu_2O/AZO Schottky junction, we demonstrate the effectiveness of forming homojunction to further exploit the potential of Cu_2O as a photocathode.

2. Experimental section

2.1. Sample preparation

The Cu foil (2 cm × 2 cm) was gently polished by sandpaper to remove the native oxide on the surface and rinsed by deionized water. Then the Cu foil was immersed in the electrochemical polishing solution (H_3PO_4: PEG–400 = 3:1, in volume ratio) with another piece of Cu foil as counter electrode. The operating voltage was 1.5 V versus counter electrode and the treatment maintained for 30 min.

The p-type Cu_2O thin films were deposited by electrodeposition from a basic solution of lactate-stabilized cupric sulfate [19]. In brief, the plating bath was 0.4 M cupric sulfate anhydrous and 3 M lactic acid in aqueous solution. Prior to deposition, the bath pH value was adjusted to 11 through addition of sodium hydroxide and the temperature of the bath was maintained at 60 °C. The electrodeposition was conducted potentiostatically in a typical three-electrode system. The as prepared Cu foil was used as working electrode while a Pt foil and an Ag/AgCl (satd. KCl) were used as counter electrode and reference electrode, respectively. The electrodeposition potential was always kept at −0.4 V vs. Ag/AgCl for 5 min. Finally, the Cu_2O/Cu electrode was rinsed by deionized water.

The n-type Cu_2O was electrodeposited on top of the previously deposited p-type Cu_2O film [5]. The deposition bath was 0.02 M cupric acetate monohydrate and 0.08 M acetic acid in aqueous solutions. Prior to deposition, the bath pH value was adjusted to 4.9 using sodium hydroxide and the temperature of the bath was maintained at 70 °C. The electrodeposition potential was always kept at +0.02 V vs. Ag/AgCl (satd. KCl) for 5 min. Afterwards, the p-n Cu_2O electrode was rinsed by deionized water and dried by flowing N_2.

For solid-state measurements, a 300 nm-thick Al film was deposited by e-beam evaporation on top of the Cu_2O film as the front contact, with the Cu substrate acting as the back contact. Two Cu wires were attached to the Al film and Cu, respectively, for electrical connection with the potentiostat.

For samples used for photoelectrochemical measurements, oxide overlayers were deposited on p-n Cu_2O electrode by a home-made ALD system. Before ALD, the electrode was dipped in the 30% hydrogen peroxide for two times to remove the residual organic contaminants during the electrodeposition and saturate the Cu_2O surface with hydroxyl groups for ALD. The ALD precursors for Zn, Al and O of AZO were diethylzinc (DEZ), trimethylaluminum (TMA) and water, which were maintained at room temperature. Each precursor was dosed for 0.1 s, followed by a 15 s nitrogen purge. AZO layer was deposited by five supercycles consisting of 1 cycle of TMA and H_2O after 40 cycles of DEZ and H_2O, at 120 °C. The TiO_2 protective layer was deposited with titanium tetraisoporpoxide (TTIP) and H_2O maintained at 50 °C and room temperature, respectively. Each precursor was dosed for 0.1 s, followed by a 10 s nitrogen purge. The process consisted of 1500 cycles.

Epoxy resin was applied before platinization to cover any exposed Cu electrode. In order to enhance the kinetics for water reduction reaction, Pt nanoparticles were deposited by galvanostatic photodeposition with a current density of $-8.5\ \mu A/cm^2$ for 15 min under simulated one sun illumination using 1 mM aqueous solution of H_2PtCl_6.

2.2. Characterization

The morphology and microstructure of the films were characterized using a field-emission scanning electron microscopy (FESEM) (Hitachi S-4800, 5 kV) with energy-dispersive X-ray spectrum (EDX). The crystal structure was evaluated with X-ray diffractometer (D/MAX-2500), using Cu Kα radiation (λ = 1.5416 Å) at 40 kV and 140 mA. XRD spectra were acquired over a 2θ range of 20–80° at a scanning speed of 8° per minute. Time-resolved PL spectroscopy was performed on Fluorolog-3 of HORIBA Jobin Yvon. Solution concentration was detected by ICP-MS (7700x, Agilent).

2.3. Photoelectrochemical measurements

The photoelectrochemical performance of the photocathodes were evaluated in a three-electrode configuration, with the photocathodes as the working electrode, a platinum foil (2 cm × 2 cm) as the counter electrode and Ag/AgCl/sat. KCl as the reference electrode. The linear sweep voltammetry (J-V plots) and chronoamperometry (stability plots) were carried in an electrolyte solution of 0.5 M Na_2SO_4 and 0.1 M KH_2PO_4 at pH 4.15, under simulated AM 1.5G illumination (100 mW/cm^2) using an Ivium Potentiostat/Galvanostat. The scan rate for the linear sweep voltammetry was 10 mV/s and the stability was tested at a fixed electrode potential of 0 V versus RHE. And the H_2 product was collected and analyzed by an on-line gas chromatograph (GC 2060, Ramiin) with a thermal conductivity detector (TCD) using Ar as the carrier gas. Prior to the test, the air tightness of the system was examined. The pressure of the system maintained at the range of 0.1 kPa–0.4 kPa (absolute pressure) in five hours, indicating the good air tightness of our system. Prior to the test, the electrolyte was purged with nitrogen gas to remove oxygen and thus eliminate erroneous signals arising from oxygen reduction. During the test, the electrolyte was continuously stirred during each measurement to detach the hydrogen from the surface of the TiO_2 protective layer. Mott-Schottky plots were obtained in a 0.2 M K_2SO_4 solution (pH 5.6) at 10 kHz. The charge carrier densities (N_A, cm^{-3}) of Cu_2O photocathodes can be obtained from Mott-Schottky

plots and the equation of $1/C^2 = 2/(e\varepsilon_r\varepsilon_o N_A) \times (E-E_{fb}-kT/e)$, where C is the capacitance of the space charge region, $e = 1.60 \times 10^{-19}$C, $\varepsilon_r = 7.5$ is the relatively permittivity of Cu_2O, $\varepsilon_0 = 8.85 \times 10^{-14}$ F/cm is the permittivity of vacuum, E is the electrode applied potential, E_{fb} is the flat band potential, k is the Boltzmann constant, and T is the absolute temperature. The solar energy conversion efficiencies (η) were calculated according to the following equation $\eta = (V_{app} \times J_{ph})/P \times 100\%$, where V_{app} is the applied potential (vs. RHE), J_{ph} is the photocurrent (mA/cm^2) under AM 1.5G irradiation and P is the irradiance of the AM 1.5G (100 mW/cm^2). The incident photon-to-current conversion efficiencies (IPCE) were measured under monochromatic illumination at 0 V versus RHE using the equation IPCE% = $[J_{ph}(mA/cm^2) \times 1240]/[P(mW/cm^2) \times \lambda(nm)] \times 100$. The Faradaic efficiency (FE) for the hydrogen product was calculated according to the following equation FE(%) = mol products × number of electrons needed for conversion/moles of electrons passed × 100%.

3. Results and discussion

The p-Cu_2O thin films were deposited on Cu foils by electrodeposition from a basic solution of lactate-stabilized cupric sulfate, without using Au layer as the back contact. Following this step, an n-Cu_2O thin film was deposited on top of the as-prepared p-type Cu_2O layer to form a homojunction in the weakly acidic solution of cupric acetate. The bath pH was adjusted to 4.9 and the temperature was maintained at 70 °C. The electrodeposition potential was always kept at

+0.02 V vs. Ag/AgCl (satd. KCl). The p-type conductivity in Cu_2O is due to the copper vacancies. The acid solution can suppress copper vacancies and populate oxygen vacancies in Cu_2O, thus forming n-type films [20]. The p-n Cu_2O homojunction has larger built-in potential and less interface defects than the p-Cu_2O/AZO Schottky junction, which may greatly improve the water splitting performance. In addition, the p-n homojunction photocathode is protected by ALD-grown TiO_2 layer with AZO bonding layer, and activated with electrodeposited Pt for hydrogen evolution. So far, the utilization of consecutively electrodeposited p-n Cu_2O homojuncion is limited to solid-state photovoltaic devices, due to the fact that n-type Cu_2O is extremely unstable in aqueous electrolytes. Owing to the dense TiO_2 protective layer enabled by ALD, this p-n homojunction eventually presents its potential in photoelectrochemical water splitting in this study.

3.1. Homogeneous p-n Cu_2O junction photocathodes

The morphology and perspective illustrations of different Cu_2O samples are shown in Fig. 1. The p-Cu_2O film show a cubic morphology (Fig. 1a). Upon the second electrodeposition for n-type layer, most of the p-Cu_2O surface could be covered by n-Cu_2O (Fig. 1b). After ALD of AZO and TiO_2, the morphology of Cu_2O photocathodes remained unchanged (Fig. 1c and d). The cross-sectional scanning electron microscopy (SEM) images of the Cu_2O homojunction show that the p-Cu_2O layer is about 1000 ± 70 nm thick, and the n-Cu_2O layer is about 500 ± 50 nm thick (Fig. S1). The ALD of AZO and TiO_2 was carried out
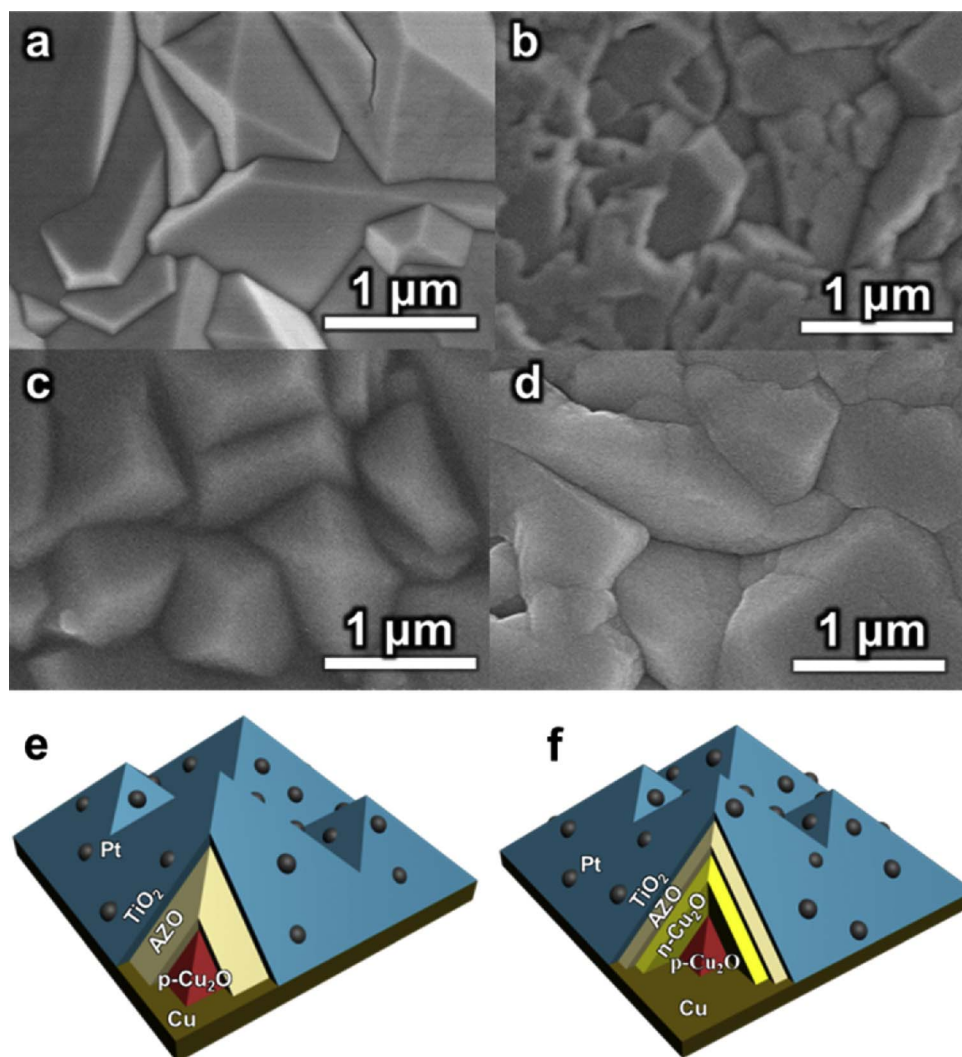

Fig. 1. Top view SEM images of (a) p-Cu_2O, (b) p-n Cu_2O, (c) p-Cu_2O/AZO/TiO_2, (d) p-n Cu_2O/AZO/TiO_2; Three-dimensional perspective views of (e) p-Cu_2O/AZO/TiO_2/Pt, (f) p-n Cu_2O/AZO/TiO_2/Pt.
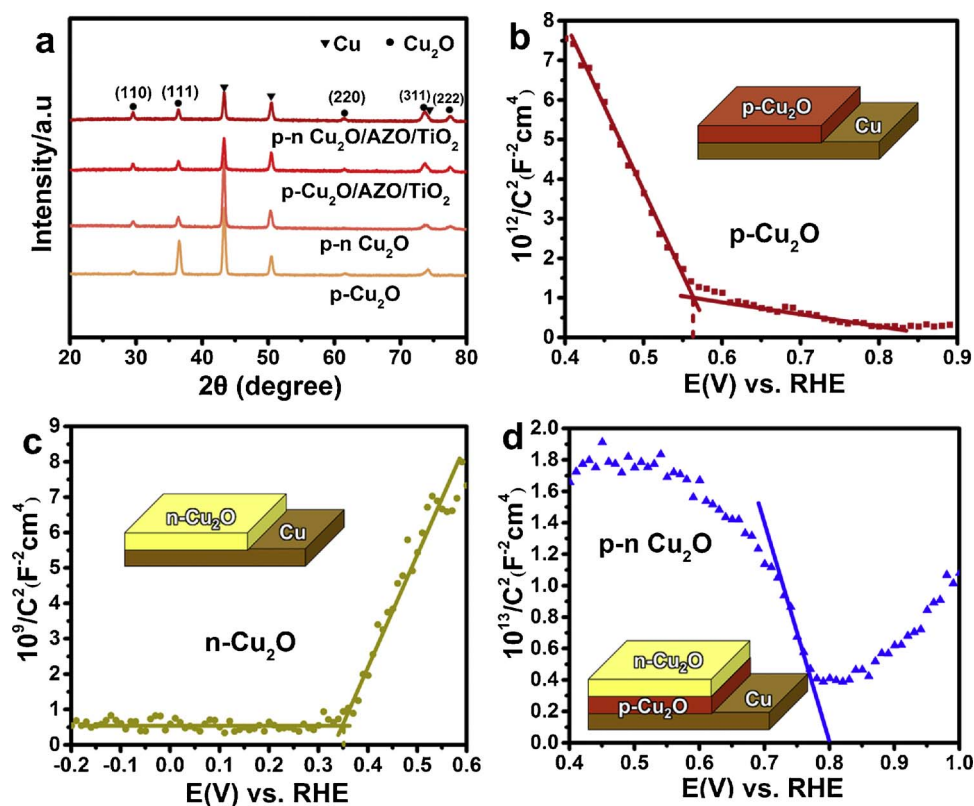
at 120 °C and 150 °C, respectively. The ellipsometric thickness of AZO and TiO$_2$ are both 30 nm measured from Si monitor substrates.

To further evaluate the phase of the photocathodes, grazing incidence X-ray diffraction (GIXRD) measurements were performed (Fig. 2a). XRD peaks of Cu$_2$O on Cu electrodes could be obtained, exhibiting a predominant (111) orientation. The absence of AZO and TiO$_2$ signals is due to their thin thickness and low crystallinity. Mott-Schottky plots were obtained to investigate the conductive type of as-prepared Cu$_2$O films without AZO and TiO$_2$ layers. For p-type Cu$_2$O, the negative slope of the plot can be obtained (Fig. 2b), while the positive slope indicates the n type conductivity (Fig. 2c) [21]. The "V-shaped" behavior of the Mott-Schottky plot was observed for the p-n Cu$_2$O homojunction film (Fig. 2d), which could be interpreted as two capacitors in series, one corresponding to the p-Cu$_2$O/n-Cu$_2$O interface and the other to the n-Cu$_2$O/electrolyte interface [22]. The charge carrier concentration of Cu$_2$O electrode was calculated from the Mott-Schottky measurement (Table S1). To further confirm the n-type conductivity of Cu$_2$O, we fabricated Cu/Cu$_2$O/Al metal-insulator-metal (MIM) layer stacks for solid-state current-voltage (J-V) measurements. When the insulating layer is Cu$_2$O p-n junction, the MIM capacitor displays

rectifying characteristics, while the MIM capacitor with p-Cu$_2$O as the insulating layer exhibits ohmic characteristics (Fig. 3a), which verifies the n-type conductivity of the Cu$_2$O top layer. Meanwhile, the photoelectrochemical J-V curve of n-Cu$_2$O (without underlying p-Cu$_2$O) in direct contact with the electrolyte presents an anodic photocurrent, indicating the n-type conductivity of this layer (Fig. 3b).

The built-in potential (V$_{bi}$) of homogeneous Cu$_2$O p-n junction can be calculated according to the Mott-Schottky plot [23]. A linear fit of the region corresponding to the Cu$_2$O p-n junction (Fig. 2d, blue solid line) indicates that the V$_{bi}$ is 0.8 V. The theoretical V$_{bi}$ of the Cu$_2$O/ZnO heterojunction is 0.7 V according to the Fermi level offset between ZnO and Cu$_2$O [3]. However, the actual V$_{bi}$ of Cu$_2$O/AZO Schottky junction is far below 0.7 V due to the interface defects which are known to influence the band bending [24,25]. Klein and co-workers have obtained a V$_{bi}$ of 0.3 V for Cu$_2$O/AZO via X-ray photoelectron spectroscopy measurements [4]. The Cu$_2$O p-n junction presents a larger V$_{bi}$ than Cu$_2$O/AZO Schottky junction due to the decrease of interfacial defects that largely release Fermi level pinning. Additionally, the V$_{bi}$ remained the same when Mott-Schottky plots were obtained with different frequencies, assuring the result that Cu$_2$O p-n homojunction always
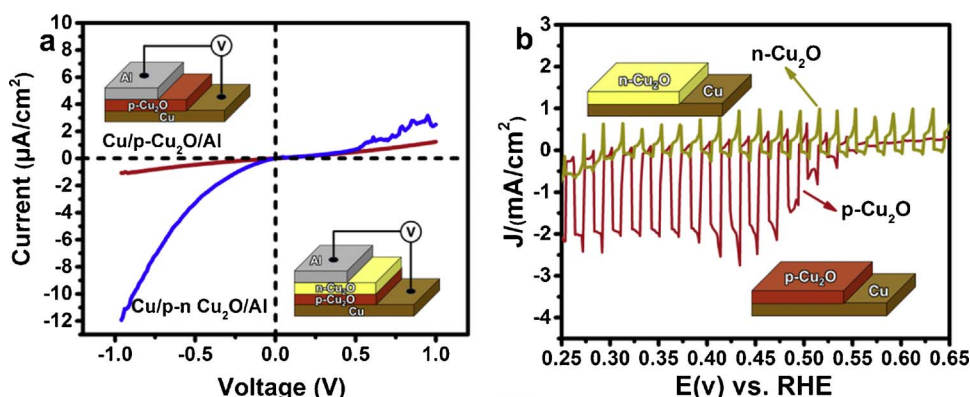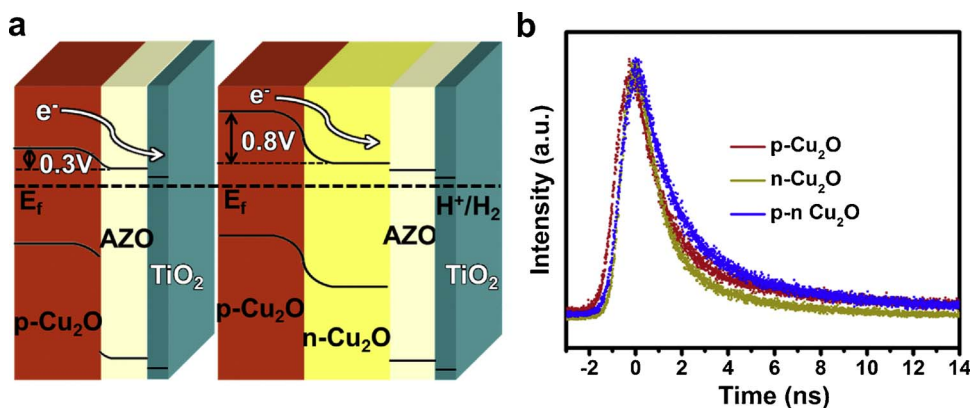
Fig. 4. (a) Schematic band diagram of a TiO$_2$-protected p-n Cu$_2$O homojunction and p-Cu$_2$O/AZO Schottky junction, at equilibrium in the dark; (b) Time-resolved PL spectra of Cu$_2$O.

exhibits a larger built-in potential than the Cu$_2$O/AZO heterojunction. Thus, the homogeneous Cu$_2$O p-n junction would form a larger splitting of the quasi-Fermi levels under illumination, which is expected to generate a larger photovoltage than the p-Cu$_2$O/AZO Schottky junction (Fig. 4a) [26,27].

In order to investigate the charge separation of the photocathodes, time-resolved photoluminescence (PL) spectroscopy was employed to monitor the fluorescence decay (Fig. 4b). The electrons and holes with long lifetimes would show slow PL decay, indicating efficient charge separation [28]. The experimental time-resolved PL intensity decay I(t) is analysed by using the following multi-exponential model [29]:

$$I(t) = b + \sum_{i=1}^{n} \alpha_i \exp(-t/\tau_i)$$

where τ_i (excited-state luminescence decay times) and α_i (pre-exponential factors) are parameters to be fitted, and b is a baseline correction parameter. The average decay time, $< \tau >$, could be calculated from

$$<\tau> = \frac{\sum_{i=1}^{n} \alpha_i \tau_i^2}{\sum_{i=1}^{n} \alpha_i \tau_i}$$

The fractional contribution f_i of each decay component was estimated by

$$f_i = \frac{\alpha_i \tau_i}{\sum_{j=1}^{n} \alpha_j \tau_j}$$

The Cu$_2$O samples were excited at 280 nm, and the PL was monitored at 535 nm. The p-n Cu$_2$O shows slower PL decay compared with p-Cu$_2$O and n-Cu$_2$O (Table 1 and Supplementary Table S2), confirming the enhanced charge separation, which could be attributed to the p-n Cu$_2$O homojunction that establishes an improved internal electric field [30]. Thus, the p-n homojunction photoelectrode is expected to present a higher activity than the Schottky heterojunction counterpart due to the enhanced interfacial charge separation, which is originated from the improved internal electric field.

3.2. Photoelectrochemical hydrogen evolution properties

Upon forming homogeneous p-Cu$_2$O/n-Cu$_2$O junction, the TiO$_2$-protected photocathodes exhibited noticeably improved photoelectrochemical performance (Fig. 5a). A positive onset potential of 0.7 V vs. RHE (defined as the potential where photocathodic current reaches 0.1 mA/cm^2 under AM 1.5G illumination) could be reached, with a 0.4 V positive shift compared to the p-Cu$_2$O/AZO Schottky junction. Meanwhile, a photocurrent of 4.30 mA/cm^2 at 0 V vs. RHE can be reached, 4.9 times higher than the p-Cu$_2$O/AZO sample (Table 2). The J-V curves present sharp spikes in each chopping cycle, owing to the contribution of capacitive currents [31], which was caused by the existence of depletion layer in the p-Cu$_2$O/n-Cu$_2$O interface, resulting in

Table 1
Fitting of the time-resolved PL spectra of the samples.

Samples	p-Cu$_2$O	n-Cu$_2$O	p-n Cu$_2$O
Decay life times (ns)	4.37	3.09	5.14

additional capacitance in the electrode [22]. It should be noted that our Cu$_2$O/AZO photocathode exhibits inferior performance compared to some recent high performance Cu$_2$O/AZO Schottky junction electrodes prepared by electrodeposition [1,32], most likely because the expensive Au layer is not used as ohmic back contact in this study. However, the performance of our Cu$_2$O p-n homojunction photocathode without Au layer is comparable to the most efficient Cu$_2$O/AZO photocathodes reported previously (Table S3). The Cu$_2$O photocathode prepared by thermal oxidation[6,7] exhibits superb performance due to high carrier mobility [16], but this method is rather complicated and requires the removal of CuO layer on the surface. Thus, we adopt a simple electrodeposition method to fabricate Cu$_2$O electrodes without using the expensive Au layer, which will sacrifice the activity. But our Cu$_2$O in p-n homojunction and Cu$_2$O/AZO Schottky junction was fabricated with the same method, which provides a reliable comparison to demonstrate the effectiveness of forming homojunction. Upon the formation of homogeneous p-n junction, our Cu$_2$O photocathode prepared by this facile electrodeposition process presents comparable performance to those prepared by thermal oxidation (Table S3).

A maximum solar energy conversion efficiency of 0.5% is achieved at 0.35 V vs. RHE for the TiO$_2$-protected homogeneous Cu$_2$O p-n junction electrode (Fig. 5b), which is seven times as high as the maximum solar energy conversion efficiency of p-Cu$_2$O/AZO Schottky heterojunction electrode. The p-n Cu$_2$O homojunction electrode presents a much higher the incident photon-to-current conversion efficiency (IPCE) than the p-Cu$_2$O/AZO electrode (Fig. S2), suggesting the improved charge collection due to the larger built-in potential at the p-Cu$_2$O/n-Cu$_2$O interface. By integrating the IPCE over the AM 1.5G spectrum, photocurrent density values of 0.89 and 4.65 mA/cm^2 could

Table 2
Performance for different Cu$_2$O photocathodes.

Samples	Onset potential (V vs. RHE)	Photocurrent at 0 V vs.RHE (mA/cm^2)	Solar energy conversion efficiency (%)
p-Cu$_2$O/AZO/ TiO$_2$/Pt	0.3	0.87	0.07
p-Cu$_2$O/n-Cu$_2$O /AZO/ TiO$_2$/Pt	0.7	4.30	0.50

be obtained for the p-Cu$_2$O/AZO/TiO$_2$/Pt and p-n Cu$_2$O/AZO/TiO$_2$/Pt photoelectrodes, respectively (Fig. S3), which are very close to 0.87 and 4.30 mA/cm^2 at 0 V vs. RHE obtained from the J-V measurement (Fig. 5a). This indicates that the measured J-V curves using our solar simulator are consistent with the IPCE data measured by our monochromener.

3.3. Photocathode stability and faradaic efficiency

The stability of the photocathodes in 0.5 M Na$_2$SO$_4$-0.1 M KH$_2$PO$_4$ electrolyte were evaluated under continuous AM 1.5G illumination at 0 V vs. RHE. The photocurrent of bare p-Cu$_2$O electrode and the bare p-n Cu$_2$O electrode without AZO/TiO$_2$ protective layer decreased significantly at the beginning of the stability test and almost lost their entire photoactivity within 30 min (Fig. S4), which is consistent with previous reports [33]. The Cu$^+$ can be reduced to Cu^0 by electrons or oxidized to Cu^{2+} by holes because the redox potentials for the reduction and oxidation of Cu$^+$ lie within the bandgap of Cu$_2$O. The electrodes turned black due to the conversion of Cu$_2$O to Cu and CuO. To improve the stability of Cu$_2$O photocathodes in aqueous electrolytes, chemically stable oxide protective layers could be deposited by ALD. The TiO$_2$ growth follows a layer-by-layer mechanism on ZnO, while an island growth mode is expected on electrodeposited Cu$_2$O [1]. Thus, an AZO layer was introduced as a bonding layer to alter the TiO$_2$ growth mechanism to form a conformal protective layer on Cu$_2$O. The TiO$_2$ protective layer effectively prevents the Cu$_2$O layer from contacting the electrolyte solution while allowing photogenerated electrons to transfer through owing to its appropriate conduction band position. It is noted that the homogeneous Cu$_2$O p-n junction photocathode shows worse stability than the Cu$_2$O/AZO Schottky junction electrode (Fig. 5c). This may be because that n-Cu$_2$O is more vulnerable to corrosion and oxygen deficiency in n-Cu$_2$O is affected by water molecules through pinholes in TiO$_2$. The detachment of Pt cocatalyst is aslo a possible reason. After stability test, the electrolyte solution was detected by inductively coupled plasma mass spectrometry (ICP-MS) measurement, which revealed the existence of dissolved copper and other ions in the solution (Table

S4). Therefore, we explored thicker TiO$_2$ layers to extend our device lifetime by reducing the pinholes in the protective film. The stability of p-n Cu$_2$O photocathode could be largely enhanced when a 100 nm thick TiO$_2$ protective layer is utilized (Fig. S5).

The amounts of hydrogen produced from the photocathodes under AM 1.5G were measured at 0 V vs. RHE in 0.5 M Na$_2$SO$_4$-0.1 M KH$_2$PO$_4$ electrolyte (Fig. 5d). The Faradaic efficiencies (FE) of p-Cu$_2$O/AZO/TiO$_2$/Pt and p-n Cu$_2$O/AZO/TiO$_2$/Pt photoelectrodes are 84.78% and 67.24%, respectively. The low FE is due to the instability of the photocathodes, since the ALD-grown TiO$_2$ protective layer is not completely pinholes free, which requires further enhancement.

4. Conclusions

In conclusion, we demonstrate the successful construction of a homogeneous p-n Cu$_2$O junction photocathode for efficient water splitting by a facile electrodeposition without using Au layer as back contact. The p-n homojunction can enhance the band bending and eliminate lattice mismatch to generate a larger photovoltage and reduce the charge recombination. The longer PL decay time indicates the enhanced charge separation in the p-n Cu$_2$O homojunction. The onset potential for water reduction could be positively shifted from 0.3 to 0.7 V vs. RHE, and a cathode photocurrent of -4.30 mA/cm^2 at 0 V vs. RHE is obtained. A conformal TiO$_2$ protective layer can efficiently improve the stability of the p-n Cu$_2$O photocathode. This work reveals the importance of forming homogeneous p-n junctions over Schottky or p-n heterojunctions for solar water splitting. Many other photoactive semiconductors may adopt a similar strategy if a reliable method is developed to prepare these semiconductors with the opposite conductivity type, where new research opportunities are emerging.

Acknowledgements

Introducing Talents of Discipline to Universities (B06006) for financial support.

Appendix A. Supplementary data

Supplementary data associated with this article can be found, in the online version, at https://doi.org/10.1016/j.apcatb.2017.12.022.

References

[1] A. Paracchino, V. Laporte, K. Sivula, M. Grätzel, E. Thimsen, Nat. Mater. 10 (2011) 456–461.

[2] C. Xiang, G.M. Kimball, R.L. Grimm, B.S. Brunschwig, H.A. Atwater, N.S. Lewis, Energy Environ. Sci. 4 (2011) 1311.

[3] A.T. Marin, D. Muñoz-Rojas, D.C. Iza, T. Gershon, K.P. Musselman, J.L. MacManus-Driscoll, Adv. Funct. Mater. 23 (2013) 3413–3419.

[4] S. Siol, J.C. Hellmann, S.D. Tilley, M. Grätzel, J. Morasch, J. Deuermeier, W. Jaegermann, A. Klein, ACS Appl. Mater. Interfaces 8 (2016) 21824–21831.

[5] C.M. McShane, K.S. Choi, Phys. Chem. Chem. Phys. 14 (2012) 6112–6118.

[6] C. Li, T. Hisatomi, O. Watanabe, M. Nakabayashi, N. Shibata, K. Domen, J.-J. Delaunay, Energy Environ. Sci. 8 (2015) 1493–1500.

[7] P. Dai, W. Li, J. Xie, Y. He, J. Thorne, G. McMahon, J. Zhan, D. Wang, Angew. Chem. Int. Ed. 53 (2014) 13493–13497.

[8] J.P. Bosco, S.B. Demers, G.M. Kimball, N.S. Lewis, H.A. Atwater, J. Appl. Phys. 112 (2012) 093703.

[9] H.M. Wei, H.B. Gong, L. Chen, M. Zi, B.Q. Cao, J. Phys. Chem. C 116 (2012) 10510–10515.

[10] P. Wang, H. Wu, Y. Tang, R. Amal, Y.H. Ng, J. Phys. Chem. C 119 (2015) 26275–26282.

[11] R.E. Brandt, M. Young, H.H. Park, A. Dameron, D. Chua, Y.S. Lee, G. Teeter, R.G. Gordon, T. Buonassisi, Appl. Phys. Lett. 105 (2014) 263901.

[12] C.A.N. Fernando, S.K. Wetthasinghe, Sol. Energy Mater. Sol. Cells 63 (2000) 299–308.

[13] R. Garuthara, W. Siripala, J. Lumin. 121 (2006) 173–178.

[14] J.-N. Nian, C.-C. Tsai, P.-C. Lin, H. Teng, J. Electrochem. Soc. 156 (2009) H567.

[15] Y.C. Lee, Y.L. Chueh, C.H. Hsieh, M.T. Chang, L.J. Chou, Z.L. Wang, Y.W. Lan, C.D. Chen, H. Kurata, S. Isoda, Small 3 (2007) 1356–1361.

[16] R. Wick, S.D. Tilley, J. Phys. Chem. C 119 (2015) 26243–26257.

[17] Y. Yang, D.S. Kim, Y. Qin, A. Berger, R. Scholz, H. Kim, M. Knez, U. Gosele, J. Am. Chem. Soc. 131 (2009) 13920–13921.

[18] Y. Lin, R. Kapadia, J. Yang, M. Zheng, K. Chen, M. Hettick, X. Yin, C. Battaglia, I.D. Sharp, J.W. Ager, A. Javey, J. Phys. Chem. C 119 (2015) 2308–2313.

[19] X. Chang, T. Wang, P. Zhang, Y. Wei, J. Zhao, J. Gong, Angew. Chem. Int. Ed. 55 (2016) 8840–8845.

[20] L. Wang, M. Tao, Electrochem. Solid-State Lett. 10 (2007) H248.

[21] W. Wang, D. Wu, Q. Zhang, L. Wang, M. Tao, J. Appl. Phys. 107 (2010) 123717.

[22] T. Jiang, T. Xie, W. Yang, L. Chen, H. Fan, D. Wang, J. Phys. Chem. C 117 (2013) 4619–4624.

[23] W.A. Laban, L. Etgar, Energy Environ. Sci. 6 (2013) 3249.

[24] K.P. Musselman, A. Marin, A. Wisnet, C. Scheu, J.L. MacManus-Driscoll, L. Schmidt-Mende, Adv. Funct. Mater. 21 (2011) 573–582.

[25] Y. Nishi, T. Miyata, T. Minami, J. Vac. Sci. Technol A 30 (2012) 04D103.

[26] A. Paracchino, N. Mathews, T. Hisatomi, M. Stefik, S.D. Tilley, M. Grätzel, Energy Environ. Sci. 5 (2012) 8673.

[27] H. Tanaka, T. Shimakawa, T. Miyata, H. Sato, T. Minami, Appl. Surf. Sci. 244 (2005) 568–572.

[28] J. Zhang, M. Zhang, R.Q. Sun, X. Wang, Angew. Chem. Int. Ed. 51 (2012) 10145–10149.

[29] K. Das, S.K. De, J. Lumin. 129 (2009) 1015–1022.

[30] X. Chang, T. Wang, P. Zhang, J. Zhang, A. Li, J. Gong, J. Am. Chem. Soc. 137 (2015) 8356–8359.

[31] A. Martínez-García, V.K. Vendra, S. Sunkara, P. Haldankar, J. Jasinski, M.K. Sunkara, J. Mater. Chem.A 1 (2013) 15235.

[32] S.D. Tilley, M. Schreier, J. Azevedo, M. Stefik, M. Grätzel, Adv. Funct. Mater. 24 (2014) 303–311.

[33] W. Siripala, A. Ivanovskaya, T.F. Jaramillo, S.-H. Baeck, E.W. McFarland, Sol. Energy Mater. Sol. Cells 77 (2003) 229–237.